Available online at www.sciencedirect.com
SCIENCE DIRECT®
Chemical Physics Letters 387 (2004) 149–154
CHEMICAL PHYSICS LETTERS
www.elsevier.com/locate/cplett

Absorption-spectral features of single-walled carbon nanotubes

Yang Zhao, XiuJun Wang, Chi-Chiu Ma, GuanHua Chen *

Department of Chemistry, University of Hong Kong, Pokfulam Road, Hong Kong, PR China

Received 11 September 2003; in final form 4 February 2004

Abstract

We present a visual, intuitive connection between optical absorption line shapes and the underlying carbon nanotube structures. Within the tight-binding model, the absorption spectra can be linked directly to plots of energy contours and transition dipoles of a graphene sheet. Via two additional approaches, spectral features are shown only slightly altered by electronic correlations and σ–π orbital rehybridization. Despite dependence of electronic structures on chiral angles, it is proved that, if the tube diameter D is greater than the C–C bond length a, the absorption spectra are determined by D to the lowest order in a/D.

In 1998, White and Mintmire [1] solved a puzzle posed by Dresselhaus [2] on that the density of states (DOS) is independent of translational unit cell sizes and chiral angles of semiconducting carbon nanotubes [3]. Their discovery has been employed to interpret the absorption spectra and electron energy loss spectroscopy (EELS) of a bundle of single-walled carbon nanotubes (SWNTs) of similar sizes. The two lowest peaks were assigned to the semiconducting SWNTs and the third was attributed to the metallic tubes. The energies of the three peaks are approximately $\frac{2a}{D}|V_{pp\pi}|$, $\frac{4a}{D}|V_{pp\pi}|$ and $\frac{6a}{D}|V_{pp\pi}|$ with $V_{pp\pi}$ the p_π transfer integral between two nearest carbon atoms. These interpretations, while likely correct, has not been adequately scrutinized. Firstly, in addition to the DOS, the absorption lineshape also has a nontrivial dependence on the transition dipole moments between pairs of valence and conduction bands. A finite transition dipole projection along the direction of an external field ensures the appearance of an absorption peak which links two van Hove singularities in the DOS, while a zero or negligible transition dipole moment gives no absorption peaks even if the corresponding DOS diverges. The transition dipole moments in the entire Brillouin zone, however, have remained elusive in the literature. Secondly, the conclusion of White and Mintmire [1] was based on a simple tight-binding model which only considers explicitly the π electrons. Rehybridization of σ and π orbitals and electronic correlations [4] are known to affect the band structure, DOS and transition dipoles, and may thus lead to substantial changes of the absorption spectrum. Therefore, more realistic calculations beyond the tight-binding model are needed to examine the implications of White and Mintmire's discovery on the optical absorption. In this Letter, we start with the tight-binding model and determine the general absorption spectral features of SWNTs from plots of the conduction (valence) band contours and the transition dipole field lines of a graphene sheet. We prove that to the lowest order in a/D the absorption spectra of SWNTs are determined mainly by their diameters instead of their chiral angles within the tight-binding model. These findings are then examined by including explicitly the electronic correlations and the σ–π orbital rehybridization in the framework of the localized-density-matrix (LDM) method [5,6] and the first-principles density-functional theory (DFT) [7]. It is shown that these general spectral features persist in the presence of electron–electron Coulomb interactions and σ–π orbital rehybridization, and are thus universal.

Carbon nanotubes are simply the rolled-up graphene sheets. They are classified by their chiralities which are labeled by the chiral vector $\mathbf{C}_h = n\mathbf{a}_1 + m\mathbf{a}_2$ with $\mathbf{a}_1$ and

* Corresponding author. Fax: +85-228-571-586.
E-mail address: ghc@everest.hku.hk (GH. Chen).

0009-2614/$ - see front matter © 2004 Elsevier B.V. All rights reserved.
doi:10.1016/j.cplett.2004.02.007

$\mathbf{a}_2$ the real space unit vectors of the hexagonal graphite lattice. Consequently, their physical properties are closely related to those of the graphite [8]. In the tight-binding model where only π electrons are considered, the electronic structures of carbon nanotubes can be derived directly from that of a graphene sheet. The band spectra of a carbon nanotube are the intersects of a graphene sheet's conduction and valence energy surfaces and a set of parallel planes perpendicular to the Brillouin zone (see Fig. 1a). The hexagon in Fig. 1a is the first Brillouin zone of a graphene sheet, and the parallel lines, which are along the tubule axis **T**, are the intersects between the Brillouin zone and the set of parallel planes. The parallel lines shown in Fig. 1a are the allowed states for a (5,5) SWNT. At K points the conduction (E_c) and valence (E_v) bands join, and the energy difference $E_c - E_v$ vanishes; at Γ points $E_c - E_v$ reaches its maxima; and M points are the saddle points where the energy difference is rather flat nearby. If one of the intersects or parallel lines such as those in Fig. 1a goes through a K point in the Brillouin zone, the tube is metallic ($n - m = 3k$). Otherwise it is a semiconductor ($n - m = 3k \pm 1$). The absorption spectra of SWNTs can be similarly obtained from the optical properties of a graphene sheet via a set of graphic tools, which will be demonstrated below.

The optical responses of carbon nanotubes are highly anisotropic [5,6], and the transition dipole along the tubule axis **T** was found much larger than its component perpendicular to the tubes. We consider here only the scenario in which the external field is parallel to the tubule axis (**E**||**T**), and thus the transition occurs

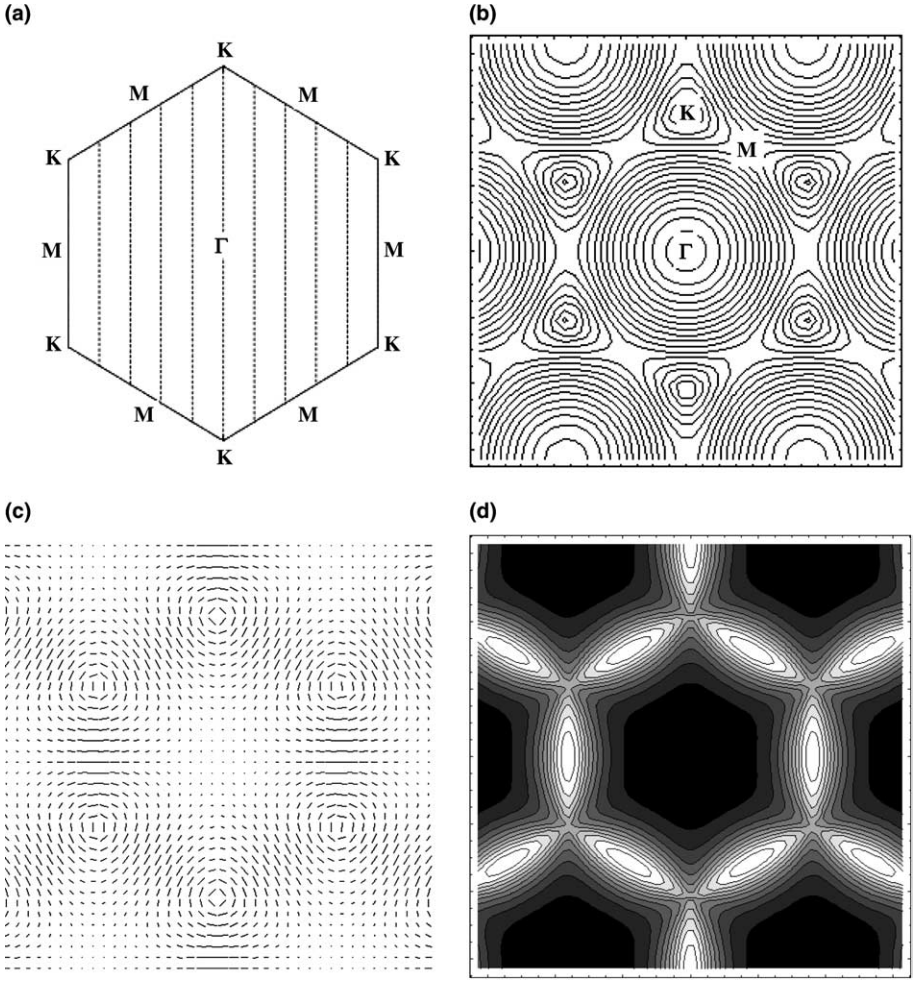

Fig. 1. (a) The first Brillouin zone of graphene sheet. The parallel lines (along the tubule axis **T**) are the intersects between the Brillouin zone and the parallel planes which are perpendicular to the Brillouin zone. They represent the allowed states for a (5,5) SWNT. (b) The contour plot of the conduction band of the graphene sheet. The circle at the center of the first Brillouin zone is the Γ point, and the six surrounding circles are the K points where the conduction and valence bands join. (c) The transition-dipole field lines of graphene in the first Brillouin zone. The orientations of the lines represent the directions of the transition dipoles at that particular **k**, and the lengths of the lines represent the sizes of the transition dipoles. The transition dipole vanishes asymptotically on approaching the Brillouin zone center. The size of transition dipole reaches its maxima on lines connecting neighboring K points. A circular pattern is found around K points. (d) The contour plot of the oscillator strength $|\mathbf{d}|^2$. The $|\mathbf{d}|^2$ maxima are located at M points (light area), and its minima, at the Γ point (dark area).

exclusively between the orbitals of the same momenta **k** [9,10]. The corresponding contribution to the absorption lineshape from excitations at the momentum **k** is determined by two factors, namely, the transition dipole projected along the tubule axis, $\mathbf{T}\cdot\mathbf{d}$, and the nanotube DOS for the corresponding conduction (valence) band at **k**, which is precisely $(\mathbf{T}\cdot\nabla_{\mathbf{k}}E_{\mathrm{c}})^{-1}$ $[(\mathbf{T}\cdot\nabla_{\mathbf{k}}E_{\mathrm{v}})^{-1}]$. In another word, the absorption intensity is proportional to $(\mathbf{T}\cdot\mathbf{d})^2(\mathbf{T}\cdot\nabla_{\mathbf{k}}E_{\mathrm{c}})^{-1}(\mathbf{T}\cdot\nabla_{\mathbf{k}}E_{\mathrm{v}})^{-1}$. Fig. 1b depicts the contour lines of the conduction band E_{c}. When the tubule axis is tangential to a contour line of E_{c} at a given **k**, $(\mathbf{T}\cdot\nabla_{\mathbf{k}}E_{\mathrm{c}})^{-1}$ diverges, and a van Hove singularity appears in the DOS. Since E_{c} and E_{v} are mirror images of each other, $(\mathbf{T}\cdot\nabla_{\mathbf{k}}E_{\mathrm{v}})^{-1}$ diverges as well at that **k**. If the transition dipole between the valence and conduction orbitals has a nonzero projection along **T** at **k**, a corresponding peak arises in the absorption spectrum. Of particular interest are *K* and *M* points in the Brillouin zone. An intersect through *K* does not cause a van Hove singularity, but adjacent intersects do as noted by White and Mintmire. For metallic SWNTs, two intersects with a spacing $\frac{2}{D}$ from the *K* point have van Hove singularities. Since the energy contours are nearly circular around the *K* point (cf. Fig. 1b), $E_{\mathrm{c}}-E_{\mathrm{v}}$ at both van Hove singularities can be approximated by $\frac{6a}{D}|V_{pp\pi}|$. For semiconducting tubes, no intersect goes through *K* points. The closest intersect to a *K* point is $\frac{2}{3D}$ from the *K* point, and the next closest is $\frac{4}{3D}$ from the *K* point; and $E_{\mathrm{c}}-E_{\mathrm{v}}$ at the two van Hove singularities are $\frac{2a}{D}|V_{pp\pi}|$ and $\frac{4a}{D}|V_{pp\pi}|$, respectively. Similarly, any intersects at the *M* points or their vicinities may lead to van Hove singularities. Since the *M* points are saddle points where $E_{\mathrm{c}}-E_{\mathrm{v}}$ are relatively flat, transition energies linking these van Hove singularities are approximately $2|V_{pp\pi}|$.

The transition dipole **d** between the valence-band wave function $|\phi^{-}(\mathbf{k})\rangle$ and the corresponding conduction-band wave function $|\phi^{+}(\mathbf{k})\rangle$ are defined as $\mathbf{d}\equiv\langle\phi^{+}(\mathbf{k})|e\mathbf{r}|\phi^{-}(\mathbf{k})\rangle$. In Fig. 1c we plot the **d** field lines. The external electric field is parallel to the intersects or the parallel lines in Fig. 1a. Except when an intersect (see Fig. 1a) is orthogonal to the **d** field line at momentum **k**, the transition dipole will have a nonzero component along the external field. Since the **d** field lines near the *K* points are, to the lowest order, circular in pattern, any intersects in its vicinity are guaranteed not to be perpendicular to the **d** field lines. It follows that *any transitions linking the van Hove singularities near the K points are allowed*. Therefore, armed with plots of the conduction (valence) band contours and the transition dipole field lines of a graphene sheet (Fig. 1b and c), we have *proven* that the lowest energy peaks in both metallic and semiconducting tubes depend mainly on the diameter; for tubes of approximately the same diameters, the two lowest energy peaks from the semiconducting tubes are about 1/3 and 2/3 in energy, respectively, when compared with the lowest energy peaks from the metal tubes. The **d** field lines near an *M* point are approximately parallel. If an intersect is perpendicular to the **d** field lines near one *M* point, due to the existence of six equivalent *M* points in the first Brillouin zone, the same set of intersects parallel to the tubule axis will not be perpendicular to the field lines near the other five *M* points. We thus expect to observe the absorption peaks attributed to transitions at the *M* points or in their vicinities with transition energies at about $2|V_{pp\pi}|$. As seen from Fig. 1d, a graphene sheet's oscillator strength which is proportional to $|\mathbf{d}|^2$ is mainly concentrated near the Brillouin zone boundaries, i.e., in areas connecting neighboring K points. Close to the Brillouin zone center, the size of the transition dipole vanishes asymptotically. Recently, Grüneis et al. [11] pointed out an intensity node in optical absorption around the *K* points in the two-dimensional Brillouin zone of graphite, which is in full agreement with the transition–dipole plot, Fig. 1c, and the contour plot of the oscillator strength, Fig. 1d. The absorption probability nodes in Fig. 2 of [11], for example, can be reproduced by simply combining Fig. 1c and d presented here.

(6,4), (8,0) and (5,5) SWNTs have similar diameters which are 6.83, 6.26 and 6.78 Å, respectively. According to the tight-binding theory, (8,0) and (6,4) are semiconductors while (5,5) is a metal. In Fig. 2a we plot the tight-binding absorption spectra of (6,4), (8,0) and (5,5) tubes. The first two groups of peaks at $0.42|V_{pp\pi}|$ ($0.48|V_{pp\pi}|$) and $0.80|V_{pp\pi}|$ ($0.83|V_{pp\pi}|$) belong to the semiconducting (6,4) [(8,0)] nanotube, and the third peak at $1.18|V_{pp\pi}|$ belongs to the metallic (5,5) tube. All three tubes have large absorption peaks near $2|V_{pp\pi}|$. The tight-binding result of Fig. 2a shows that the intensities of the two lowest semiconductor peaks and the lowest metal peak increase with peak frequencies, while experimentally, the opposite is found for bundles with similar diameters [12]. The discrepancy can be attributed to inhomogeneities in the SWNT bundles as well as electronic correlation effects.

The first two peaks of (6,4) are 0.36 and 0.68 of the lowest peak of (5,5) in energy, which are close to 1/3 and 2/3, respectively. The slight deviation stems from (1) minor departure of the $E_{\mathrm{c}}-E_{\mathrm{v}}$ contour from the circular feature near the *K* points, also known as the trigonal warping effect [13]; (2) deviation of $E_{\mathrm{c}}-E_{\mathrm{v}}$ from its linear behavior as **k** moves away from the *K* point. The trigonal warping effect is also responsible for the spread in points in the Kataura plot [14]. (8,0) has a smaller diameter so that its absorption spectrum is blue-shifted compared to that of (6,4), and its first and second peaks are 0.41 and 0.70 of the lowest peak of (5,5), respectively. The tight-binding model that has been presented so far grossly simplifies the electronic dynamics in the tubes. As earlier DFT studies have revealed, the rehybridization of σ and π orbitals and interactions

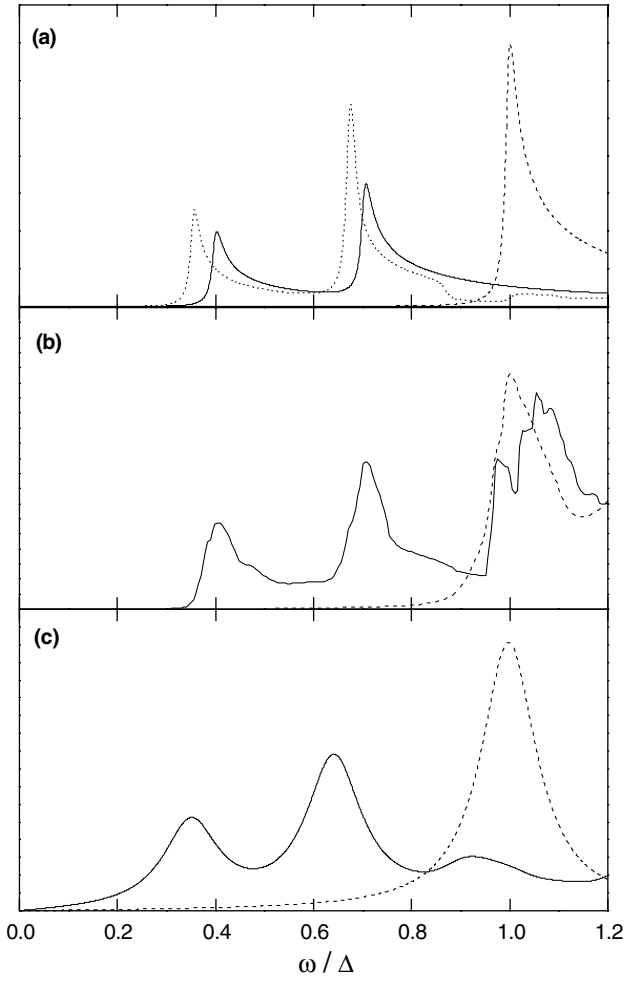

Fig. 2. The calculated absorption spectra from (a) the tight-binding model (b) DFT calculations implemented by the WIEN97 code (c) the LDM algorithm are shown for carbon nanotubes of three chiralities: (8,0) (solid lines), (5,5) (dashed lines), and (6,4) (dotted lines). (6,4) and (8,0) are semiconducting, and (5,5) is metallic. Δ labels the energy of the (5,5) SWNT's first absorption peak: (a) $\Delta = 1.18|V_{pp\pi}|$, (b) $\Delta = 2.76$ eV, (c) $\Delta = 2.34$ eV. A dephasing constant of 0.16 eV is used to generate the LDM spectra.

among π orbitals caused by the curvature of the tube lead to significant modifications of the electronic band structures [15]. It is thus plausible that the rehybridization and interactions may cause quantitative or even qualitative alternations to the absorption spectra as compared to the tight-binding results. Therefore, the general absorption spectral features emerged from the tight-binding studies need to be corroborated by more sophisticated approaches.

Using the full potential linearized plane wave method implemented in the WIEN97 code [7], we have carried out the DFT calculations for two SWNTs: (5,5) and (8,0). Exchange and correlation are included via the local spin-density approximation (LSDA) within the DFT using the Perdew–Wang parameterization [16]. Optical absorption spectra are calculated via the sum-of-states approach taking into account pairwise interband transitions [7]. The resulting absorption spectra are shown in Fig. 2b. The lowest peak of the (5,5) nanotube centers at $\sim$2.76 eV, the lowest two peaks of (8,0) are 1.12 and 1.95 eV, which are 0.41 and 0.71 of the first peak of (5,5) (2.76 eV), respectively. The DFT results of (5,5) and (8,0) tubes therefore closely resemble those from the tight-binding model. We conclude that the tight-binding spectral features survive the inclusion of σ–π orbital rehybridization as shown here by the first-principles DFT calculations.

In addition to orbital rehybridization, electronic correlations, which have not been accounted for explicitly so far, may alter the spectral features. The LDM method [5,6] which is size-consistent and based on the random phase approximation considers fully single-electron excitation configurations and partially multi-electron excitation configurations. Since all valence electrons are treated explicitly, the LDM calculation accounts for the σ–π orbital rehybridization as well. It has been used successfully to calculate the absorption spectra of SWNTs [17–19]. For instance, absorption spectra of (5,5) and (9,0) SWNTs calculated by the LDM method were found to be similar, which led to our earlier hypothesis that the SWNT absorption line shapes are mainly determined by their diameters [17–19]. The calculated LDM absorption spectra of the (8,0) and (5,5) SWNTs ($C_{128}H_{16}$ and C_{140} H_{20}, respectively) are shown in Fig. 2c. The lengths of the (8,0) and (5,5) SWNTs are approximately the same (14.92 and 14.74 Å, respectively). The PM3 Hamiltonian is employed in the LDM calculations. The first absorption peak of the (5,5) tube is at 2.34 eV. The lowest two absorption peaks for the (8,0) tube are 0.82 and 1.49 eV, which are 0.35 and 0.64 of 2.34 eV, respectively. Note the energy ratio between the lowest two absorption peaks for the (8,0) tube is 1.82. The LDM results are in approximate agreement with those from the tight-binding model. Discrepancies between the LDM and tight-binding results for the (8,0) SWNT may be attributed to electronic correlations and size effects. Due to slight mismatches between the lengths of the semiconducting and metallic SWNTs, one has to be careful about a precise comparison between the LDM metallic and semiconducting spectra (unlike the comparisons of the two lowest semiconducting peaks of the same nanotube).

As mentioned earlier in the Letter, absorption measurements and EELS lend support to the low-frequency spectral features discussed here. The combined electronic properties of SWNT bundles have been studied by the high-resolution EELS in transmission [20]. Low-energy nondispersive features were attributed to the energy separations of DOS singularities in the nanotubes. The peak appearing in the optical conductivity at 1.8 eV was argued to originate from metallic nanotubes in the bundles. Optical absorption spectroscopy on

SWNT-containing soot shows peaks between 0.6 and 3 eV which are interpreted as interband transitions between the van Hove singularities [14]. The absorption spectra of bundles of SWNTs of similar sizes have recently been measured [21]. Three low-frequency bands have been observed in the measured absorption spectra of bundles of carbon nanotubes, among which the two lowest bands were assigned to the semiconducting tubes, and the third was attributed to the conducting nanotubes. Our work here provides a rigorous proof to these interpretations of the experimental results [20,14,21,22]. Most recently, spectrofluorimetric measurements on individual SWNTs isolated in aqueous surfactant suspensions [23] delivered information on nanotube chiralities in addition to that on diameters. Those spectra revealed small deviations of absorption peaks' dependence on diameter from linear relations for semiconducting nanotubes, and this can be accounted for qualitatively by the tight-binding model. For instance, Bachilo et al. [23] observed that the energy ratios between the second and first van Hove singularities, often referred to as E_{22}/E_{11} (E_{22} and E_{11} label the second and first van Hove singularities, respectively), deviate from a central value in the opposite directions for semiconducting nanotubes with $(n-m)$ mod $3=1$ and those with $(n-m)$ mod $3=2$. This can be explained by the fact that for wave vectors sufficiently apart from the K points, the energy slope along the K–Γ lines is much steeper than that along the K–M lines (cf. Fig. 1b and 3). Although a consensus on the strength on the electron–hole interaction has yet to emerge [26], that the central value of the energy ratios E_{22}/E_{11} is found to be 1.75 [23,27] is attributed to electronic correlation effects [23,4]. In contrast to the low-frequency features, common absorption peaks attributed to the M points remain to be observed experimentally for SWNTs of various sizes and chiralities. On the Kataura plot [14,13], the width of each E_{ii} (D) curve (E_{ii} is the energy difference between the ith van Hove singularities in the conduction and valence bands) is determined by the zigzag SWNTs. Again, the zigzag SWNTs with $(n-m)$ mod $3=1$ and those with $(n-m)$ mod $3=2$ deviate from each curve center in opposite directions. Those with $(n-m)$ mod $3=1$ ($(n-m)$ mod $3=2$) form the lower (upper) bounds of the E_{ii} (D) curves.

More features in Fig. 2 of [23] can be explained intuitively by the graphical tools developed here. In Fig. 3, allowed states for a zigzag SWNT can be represented by solid horizonal lines which are perpendicular to the dotted vertical K–Γ line. As the energy slope difference on the two sides of the K point is the largest along the vertical K–Γ line among all lines going through the K point (cf. Fig. 3), zigzag SWNTs exhibit highest deviations of the energy ratios E_{22}/E_{11} from the value two. Furthermore, for zigzag SWNTs, the energy ratio E_{22}/E_{11} for the case of $(n-m)$ mod $3=2$ [$(n-m)$ mod $3=1$] is below (above) the value two, as clearly demonstrated in Fig. 3a (Fig. 3b). On the other hand, for metallic armchair nanotubes, for which the trigonal warping effect is absent due to symmetry, the allowed states are represented by lines that are parallel to the tilted solid line connecting M and K points in Fig. 3a (equivalent to the dashed parallel lines in Fig. 1a). For non-armchair metallic SWNTs, the trigonal warping effect brings about a splitting in the first absorption peak in the tight-binding model. Phonon spectra have recently been used to verify the existence of singularity splitting in the joint density of electronic states in non-armchair metallic SWNTs [24,25]. Among semiconducting nanotubes, the one with $n-m=1$ has allowed states that are on lines with the smallest deviation angle from the tilted M–K line in Fig. 3a, and consequently,

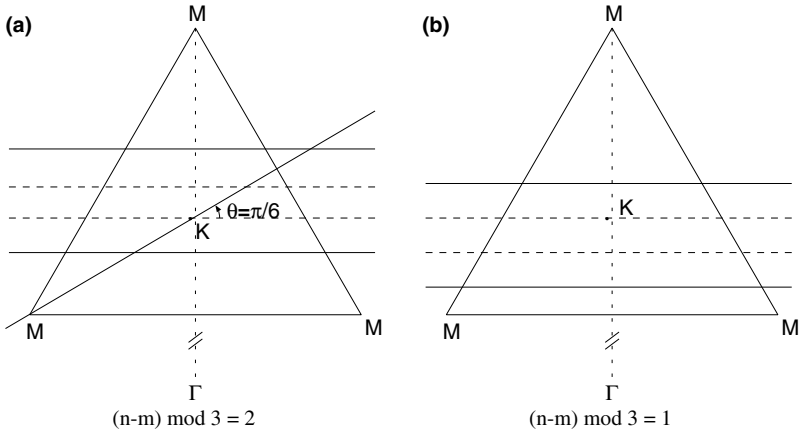

Fig. 3. Horizontal solid parallel lines are the allowed states in the Brillouin zone for (a) a zigzag nanotube with $(n-m)$ mod $3=2$, and (b) a zigzag nanotube with $(n-m)$ mod $3=1$. Dashed parallel lines divide the distance between the solid lines into 3 equal parts. One of the two dashed lines goes through the K point. The tilted solid line in (a) connecting the M and K points represents a part of allowed states for armchair nanotubes. Dotted lines connect the K and Γ points.

E_{22}/E_{11} for $n-m=1$ are closest to two. The set of parallel lines representing allowed nanotube states are not unique. Because of the sixfold symmetry of the Brillouin zone, the angle θ between the solid horizontal lines in Fig. 3a and parallel lines representing allowed states for *any* SWNT can be narrowly confined to be within $\pi/6$. This implies that the energies of allowed states for all non-armchair semiconducting SWNTs distribute asymmetrically around the K points: differing energy slopes of allowed states on the two sides of the K point cause E_{22}/E_{11} to deviate from two, the direction of which depends on whether $(n-m)$ mod 3 equals 1 or 2. As the angle θ approaches $\pi/6$ (for $n-m=1$, for example), $|E_{22}/E_{11}-2|$ minimizes. This also explains why deviation of E_{22}/E_{11} from the value two increases with n-m (and with $|\theta-\pi/6|$) as observed in [23].

There have been several theoretical attempts to examine the absorption spectra of SWNTs. Lin et al., for example, have studied the absorption spectra of bundles of SWNTs via a tight-binding model. However, they stressed the spectral differences caused by different chiral angles [9,10,28,29] while we focus on an overall intuitive connection between optical absorption line shapes and the underlying carbon nanotube structures, and on the common features dictated by the diameter to the lowest order in a/D. The common spectral features appear only when the tube diameter is much larger than the bond length, *i.e.*, $D \gg a$. Our earlier LDM study [17–19] on the 4 Å SWNTs shows that the absorption spectra of the (4,2), (3,3) and (5,0) SWNTs are distinct although their diameters are virtually the same (4.2 , 4.1, and 3.9 Å, respectively). When D is comparable to a, adjacent π orbitals overlap. The extent of the orbital overlaps depends on the orientation along which the tube is rolled up, and this leads to the spectral line shapes that are sensitive to the chiral angles. With support from both the DFT and LDM calculations we conclude that to the lowest order in a/D, the simple tight-binding model provides an accurate description of optical processes in SWNTs. The diameters of the (5,5), (6,4) and (8,0) SWNTs are modestly large compared to the C–C bond length. Greater SWNT diameters are expected to bring the DFT and LDM calculations into closer agreement with the tight-binding results. In addition to its success in describing the nanotubes' band structures, the tight-binding model provides a remarkably accurate overall account of the SWNT absorption line shapes.

To summarize, this Letter provides a visual, intuitive connection between optical absorption line shapes and the underlying nanotube structures. Calculations based on three distinctively different methods, the tight-binding model, the LDM and the DFT, result in common absorption spectral features for SWNTs with diameters much larger than the C–C bond length. These spectral features survive σ–π orbital rehybridization and electronic correlations, and are further supported by measured absorption spectra and EELS of SWNT bundles. Recently, there have been measurements on individual SWNTs in aqueous surfactant suspensions which provide information that are sensitive to both SWNT chiralities and diameters. More stringent tests on theoretical models will soon be available from Raman and luminescence measurements which are being carried out at the single-nanotube level.

Acknowledgements

This work is supported by the Hong Kong Research Grant Council (RGC) and the Committee for Research and Conference Grants (CRCG) of the University of Hong Kong.

References

[1] C.T. White, J.W. Mintmire, Nature 394 (1998) 29.
[2] M.S. Dresselhaus, Nature 391 (1998) 19.
[3] J.W.G. Wildöer et al., Nature 391 (1998) 59.
[4] C.L. Kane, E.J. Mele, Phys. Rev. Lett. 90 (2003) 207401.
[5] S. Yokojima, G.H. Chen, Chem. Phys. Lett. 300 (1999) 540.
[6] W.Z. Liang, S. Yokojima, D.H. Zhou, G.H. Chen, J. Phys. Chem. A 104 (2000) 2445.
[7] P. Blaha, K. Schwarz, J. Luitz, WIEN97, ISBN 3-9501031-0-4 (1999).
[8] R. Saito, G. Dresselhaus, M.S. Dresselhaus, Physical Properties of Carbon Nanotubes, Imperial College Press, 1998.
[9] M.F. Lin, W.K. Shung, J. Phys. Soc. Jpn. 66 (1997) 3294.
[10] M.F. Lin, Phys. Rev. B 62 (2000) 13153.
[11] A. Grüneis et al., Phys. Rev. B 67 (2003) 165402.
[12] O. Jost et al., Appl. Phys. Lett. 75 (1999) 2217.
[13] R. Saito, G. Dresselhaus, M.S. Dresselhaus, Phys. Rev. B 61 (2000) 2981.
[14] H. Kataura et al., Synth. Met. 103 (1999) 2555.
[15] X. Blase, L.X. Benedict, E.L. Shirley, S.G. Louie, Phys. Rev. Lett. 72 (1994) 1878.
[16] J.P. Perdew, Y. Wang, Phys. Rev. B 45 (1992) 13244.
[17] W.Z. Liang, X.J. Wang, S. Yokojima, G.H. Chen, J. Am. Chem. Soc. 122 (2000) 11129.
[18] W.Z. Liang, S. Yokojima, M.F. Ng, G.H. Chen, G.Z. He, J. Am. Chem. Soc. 123 (2001) 9830.
[19] W.Z. Liang, G.H. Chen, Z.M. Li, Z.K. Tang, Appl. Phys. Lett. 80 (2002) 3415.
[20] T. Pichler et al., Phys. Rev. Lett. 80 (1998) 4729.
[21] Z.M. Li et al., Phys. Rev. Lett. 87 (2001) 127401.
[22] X. Liu et al., Phys. Rev. B 66 (2002) 045411.
[23] S.M. Bachilo et al., Science 298 (2002) 2361.
[24] A.G. Souza Filho et al., Chem. Phys. Lett. 354 (2002) 62.
[25] Ge.G. Samsonidze et al., Phys. Rev. Lett. 90 (2003) 027403.
[26] A. Hartschuh et al., Science 301 (2003) 1354.
[27] M.J. O'Connell et al., Science 297 (2002) 593.
[28] J. Jiang, J. Dong, D.Y. Xing, Phys. Rev. B 59 (1999) 9838.
[29] H.J. Liu, C.T. Chan, Phys. Rev. B 66 (2002) 115416.